Electrostatic potential between charged particles at an oil-water interface: Supporting Information

Alexander Morozov, Iain Muntz, Job H. J. Thijssen and Davide Marenduzzo*
SUPA School of Physics and Astronomy,
The University of Edinburgh, Edinburgh, EH9 3FD, Scotland, United Kingdom
* *Electronic address: dmarendu@ph.ed.ac.uk*

Interfacial potential for a 3-dimensional system: Debye-Hückel exact calculation

The interaction potential between two charged particles (each of charge Q) at a flat interface between two dielectric media – for instance water and oil – with dielectric permittivities ϵ_1 and ϵ_2 respectively, can be worked out by following [1, 2], as done in the main text. The potential is given in terms of an integral involving special functions, as follows,

$$U(r) = \frac{Q^2}{2\pi r}\int_0^\infty dx \frac{xJ_0(x)}{\epsilon_1\sqrt{\kappa_1^2 r^2 + x^2} + \epsilon_2\sqrt{\kappa_2^2 r^2 + x^2}}. \tag{S1}$$

where J_0 is the zero-th order Bessel function of the first kind. Note that κ_1^{-1} and κ_2^{-1} are the Debye length in the first and second phase. For a water/oil interface, typical parameters may be $\kappa_1 \sim 10\kappa_2$ and $\epsilon_1 \sim 40\epsilon_2$ (these are relevant, for instance, to the case where the oil is dodecane [4]).

We want to find the asymptotic behaviour ($r \to \infty$) of the potential. To do so, we need the asymptotic behaviour of

$$I = \int_0^\infty dx \frac{xJ_0(x)}{\epsilon_1\sqrt{\kappa_1^2 r^2 + x^2} + \epsilon_2\sqrt{\kappa_2^2 r^2 + x^2}}. \tag{S2}$$

Tailoring the procedure in [2] to our system, we multiply the numerator and denominator in the integral in I by $\epsilon_1\sqrt{\kappa_1^2 r^2 + x^2} - \epsilon_2\sqrt{\kappa_2^2 r^2 + x^2}$ to obtain

$$I = \frac{1}{\epsilon_1^2 - \epsilon_2^2}\left(\epsilon_1 I_1 - \epsilon_2 I_2\right), \tag{S3}$$

where

$$I_i = \int_0^\infty dx \frac{xJ_0(x)\sqrt{\kappa_i^2 r^2 + x^2}}{\alpha r^2 + x^2}, \tag{S4}$$

with $i = 1, 2$ and

$$\alpha = \frac{\epsilon_1^2\kappa_1^2 - \epsilon_2^2\kappa_2^2}{\epsilon_1^2 - \epsilon_2^2}. \tag{S5}$$

Let us now introduce $\delta_i \equiv \alpha - \kappa_i^2$, explicitly given by

$$\begin{aligned}\delta_1 &= \frac{\epsilon_2^2(\kappa_1^2 - \kappa_2^2)}{\epsilon_1^2 - \epsilon_2^2} \\ \delta_2 &= \frac{\epsilon_1^2(\kappa_1^2 - \kappa_2^2)}{\epsilon_1^2 - \epsilon_2^2}.\end{aligned} \tag{S6}$$

Taylor-expanding I_i with respect to δ_i, we obtain

$$I_i = \sum_{m=0}^\infty (-1)^m(\delta_i r^2)^m \int_0^\infty dx \frac{xJ_0(x)}{\left(\kappa_i^2 r^2 + x^2\right)^{m+1/2}}. \tag{S7}$$

The integrals in these series were discussed in [2]. The resulting expression for I_i is given by

$$I_i = \sum_{m=0}^\infty (-1)^m(\delta_i r^2)^m \frac{2^{1/2-m}}{\Gamma(m+1/2)}\frac{K_{m-1/2}(\kappa_i r)}{(\kappa_i r)^{m-1/2}} = \sqrt{2\kappa_i r}\sum_{m=0}^\infty (-1)^m\left(\frac{\delta_i}{4\kappa_i^2}2\kappa_i r\right)^m \frac{K_{m-1/2}(\kappa_i r)}{\Gamma(m+1/2)}, \tag{S8}$$

where Γ denotes the Γ function [3]. Now we separate the term with $m = 0$ (which gives a screened monopole behaviour) and shift the index from m to $\mu + 1$, to get

$$I_i = \sqrt{2\kappa_i r}\left[\frac{K_{-1/2}(\kappa_i r)}{\sqrt{\pi}} - \sum_{\mu=0}^{\infty}(-1)^{\mu}\left(\frac{\delta_i}{4\kappa_i^2}2\kappa_i r\right)^{\mu+1}\frac{K_{\mu+1/2}(\kappa_i r)}{\Gamma(\mu+3/2)}\right]. \tag{S9}$$

We next use the series representation of the half-integer modified Bessel function of the second kind [3],

$$K_{\mu+1/2}(z) = e^{-z}\sqrt{\frac{\pi}{2z}}\sum_{p=0}^{\mu}\frac{(\mu+p)!}{p!(\mu-p)!}\frac{1}{(2z)^p}. \tag{S10}$$

This gives

$$I_i = \sqrt{2\kappa_i r}\left[\frac{K_{-1/2}(\kappa_i r)}{\sqrt{\pi}} - e^{-\kappa_i r}\sqrt{\frac{\pi}{2\kappa_i r}}\sum_{\mu=0}^{\infty}\sum_{p=0}^{\mu}(-1)^{\mu}\left(\frac{\delta_i}{4\kappa_i^2}\right)^{\mu+1}(2\kappa_i r)^{\mu+1-p}\frac{(\mu+p)!}{p!(\mu-p)!}\,\frac{1}{\Gamma(\mu+3/2)}\right]. \tag{S11}$$

Now, we change the order of summation in the two series,

$$I_i = \sqrt{2\kappa_i r}\left[\frac{K_{-1/2}(\kappa_i r)}{\sqrt{\pi}} - e^{-\kappa_i r}\sqrt{\frac{\pi}{2\kappa_i r}}\sum_{p=0}^{\infty}\sum_{\mu=p}^{\infty}(-1)^{\mu}\left(\frac{\delta_i}{4\kappa_i^2}\right)^{\mu+1}(2\kappa_i r)^{\mu+1-p}\frac{(\mu+p)!}{p!(\mu-p)!}\,\frac{1}{\Gamma(\mu+3/2)}\right]. \tag{S12}$$

The inner series can be re-summed, to finally get

$$I_i = e^{-\kappa_i r} - e^{-\kappa_i r}\frac{r\delta_i}{\kappa_i}\sum_{p=0}^{\infty}\frac{(-1)^p}{2p+1}\left(\frac{\delta_i}{\kappa_i^2}\right)^p {}_1F_1\left(2p+1;\frac{3}{2}+p;-\frac{r\delta_i}{2\kappa_i}\right), \tag{S13}$$

where ${}_1F_1$ is the confluent hypergeometric function of the first kind [3].

Its asymptotic behaviour (for large $\frac{r\delta_i}{2\kappa_i} \equiv z$) is given by [3]

$$\begin{aligned}{}_1F_1(a;b;-z) \sim \frac{\Gamma(b)}{\Gamma(a)}e^{-z}(-z)^{a-b}\left[1 - \frac{(a-1)(a-b)}{z} + \frac{(a-2)(a-1)(a-b-1)(a-b)}{2z^2} + \cdots\right] + \\ \frac{\Gamma(b)}{\Gamma(b-a)}\frac{1}{z^a}\left[1 + \frac{a(a-b+1)}{z} + \frac{a(a+1)(a-b+1)(a-b+2)}{2z^2} + \cdots\right].\end{aligned} \tag{S14}$$

The first sum is subdominant, if the second one exists, and for our combination of indices, it does. Therefore, we obtain the following asymptotic series (valid for $r \to \infty$),

$$I_i \sim e^{-\kappa_i r} - e^{-\kappa_i r}\left[1 + \frac{\kappa_i}{r\delta} + \frac{3\kappa_i^2}{r^2\delta^2} + \frac{1}{r^2\delta} + \mathcal{O}\left(\frac{1}{r^3}\right)\right] = -e^{-\kappa_i r}\left[\frac{\kappa_i}{r\delta} + \frac{3\kappa_i^2}{r^2\delta^2} + \frac{1}{r^2\delta} + \mathcal{O}\left(\frac{1}{r^3}\right)\right]. \tag{S15}$$

Consequently, as the integral I is dominated by the behaviour of I_2 for $r \to \infty$ (as $\kappa_2 < \kappa_1$ for a water/oil interface), we obtain that

$$I = \frac{1}{\epsilon_1^2 - \epsilon_2^2}\left(\epsilon_1 I_1 - \epsilon_2 I_2\right) \sim e^{-\kappa_2 r}\left[\frac{\epsilon_2\kappa_2}{\epsilon_1^2(\kappa_1^2-\kappa_2^2)r} + \frac{3\epsilon_2(\epsilon_1^2-\epsilon_2^2)\kappa_2^2}{\epsilon_1^4(\kappa_1^2-\kappa_2^2)^2 r^2} + \frac{\epsilon_2}{\epsilon_1^2(\kappa_1^2-\kappa_2^2)r^2}\right]. \tag{S16}$$

The numerical solution of I is compared to this approximation in Fig. S1.

The corresponding asymptotic leading behaviour for the interaction potential U is

$$U(r) \sim \frac{Q^2}{2\pi}\frac{\epsilon_2\kappa_2}{\epsilon_1^2(\kappa_1^2-\kappa_2^2)}\frac{e^{-\kappa_2 r}}{r^2}, \tag{S17}$$

which decays faster than a screened monopole with decay constant κ_2.

For a generic oil-water interface, we can consider that $\epsilon_2 \ll \epsilon_1$ and that $\kappa_2 \ll \kappa_1$. In this limit, as done in the text, it is useful to write the potential as a sum of three contribution, a screened monopole one, a "screened dipole" term $\sim \frac{e^{-\kappa_2 r}}{r^3}$, and a term $\frac{e^{-\kappa_2 r}}{r^2}$, as follows,

$$U(r) \simeq \frac{Q^2}{2\pi\epsilon_1}\frac{e^{-\kappa_1 r}}{r} + \frac{Q^2\epsilon_2}{2\pi\epsilon_1^2\kappa_1^2}\frac{e^{-\kappa_2 r}}{r^3} + \frac{Q^2\epsilon_2\kappa_2}{2\pi\epsilon_1^2\kappa_1^2}\frac{e^{-\kappa_2 r}}{r^2}. \tag{S18}$$

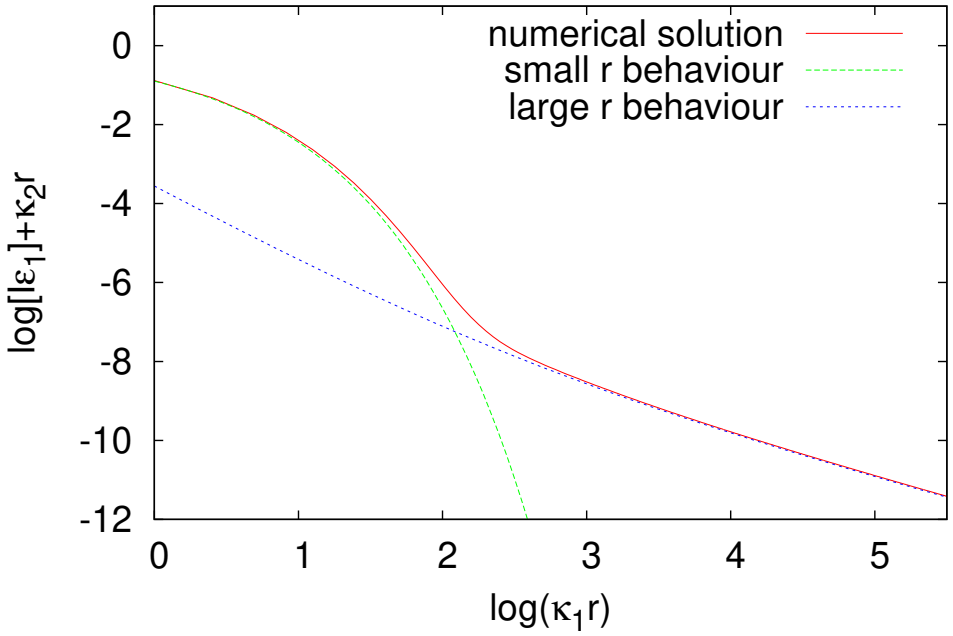

FIG. S1: Plot of the numerical solution of $\log(I\epsilon_1 e^{\kappa_2 r})$ versus $\log(\kappa_1 r)$, showing the crossover between small r behaviour, corresponding to a screened monopole with decay constant κ_1, and a large r behaviour, described by Eq. (S16). Parameters are: $\kappa_1 = 10\kappa_2$, $\epsilon_1 = 40\epsilon_2$, relevant for a water-oil interface.

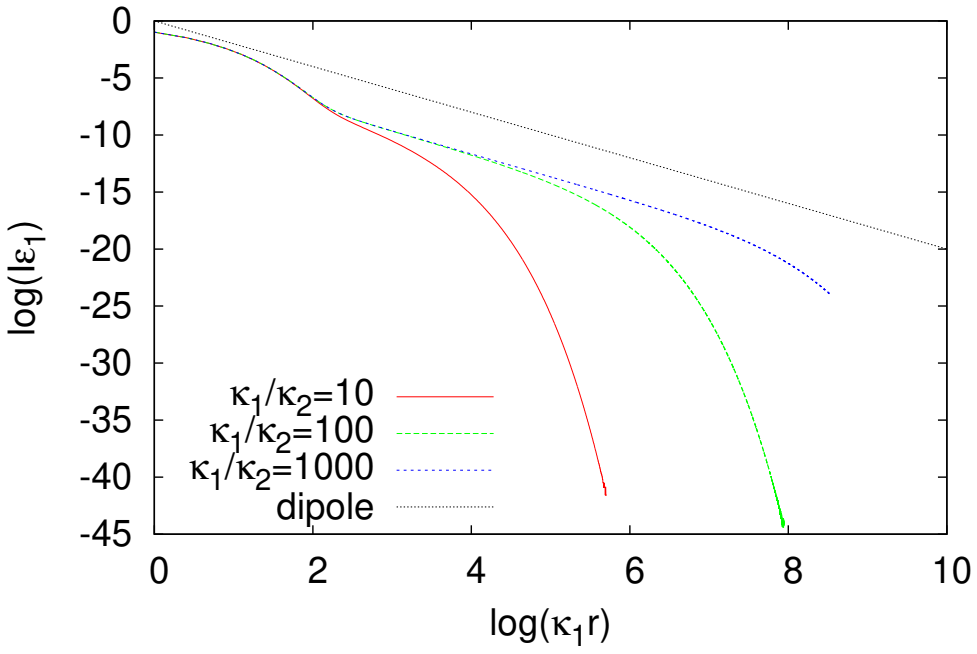

FIG. S2: Plot of the numerical solution of $\log(I\epsilon_1)$ versus $\log(\kappa_1 r)$, for different values of κ_2, showing an intermediate dipole-like decay only for very small κ_2. Curves are calculated with $\epsilon_1 = 40\epsilon_2$.

The screened monopole contribution dominates at small r, whereas the $\frac{e^{-\kappa_2 r}}{r^2}$ is the asymptotic contribution, which

dominates for $r \to \infty$. The screened dipole term $\sim \frac{e^{-\kappa_2 r}}{r^3}$ is the one which gives the dipolar interaction if $\kappa_2 = 0$. For finite κ_2, it can be seen at intermediate values of r, but only under some conditions. Taking $\epsilon_1 = 40\epsilon_2$, Fig. S2 shows that an apparent dipolar contribution can only be seen if $\kappa_1 \gg 10\kappa_2$.

Although in the main text we have considered the case of an interface with no mobile ions, the case of a salty interface, with interfacial Debye length equal to κ_3, can be studied by using the methods in [5], where it was shown that it can be dealt with as a modified boundary condition at $z = 0$ (the plane of the interface). The resulting interfacial potential is given by the following integral,

$$\phi(r) = \frac{Q}{4\pi^2} \int d^2\mathbf{q} \frac{e^{i\mathbf{q}\cdot\mathbf{r}}}{\epsilon_1\sqrt{\kappa_1^2+q^2} + \epsilon_2\sqrt{\kappa_2^2+q^2} + \epsilon_1\kappa_3}. \tag{S19}$$

The singularity at $q = i\kappa_2$ has the same structure as the one considered in the main text with no mobile ions at the interface, so that the asymptotic behaviour will also be the same.

Interfacial potential for a 3-dimensional system: non-linear Poisson-Boltzmann simulations

The Debye-Hückel theory we have just presented is valid for point-like particles, and in the limit in which $\frac{Ze_0\phi}{k_BT} \ll 1$ (where Z is the valence of the ionic species in solutions) which is used to linearise the Poisson-Boltzmann (PB) equation. To see how these two assumptions affect the results, we have also numerically solved the full non-linear PB equation for a colloidal particle of size R at an interface between two media with finite but distinct Debye lengths, in the case of monovalent salt, $Z = 1$. The PB equation for this problem can be written down as follows

$$\nabla \cdot \left(\epsilon(\mathbf{r}, z)\nabla\tilde{\phi}\right) - \epsilon(r, z)\kappa^2(r, z)\sinh(\tilde{\phi}) = -\rho(r, z) \tag{S20}$$

where $\tilde{\phi} \equiv \frac{e_0\phi}{k_BT}$ is the dimensionless electrostatic potential, and $\rho(r, z)$ is the charge distribution introduced by the colloidal particles, while other symbols are as defined in the main text. For spherical particles, the problem has cylindrical symmetry, hence the only dependence on $\mathbf{r}$ of physical quantities is through $r = |\mathbf{r}|$.

We have used four different choices for the functional form of $\rho(r, z)$, or equivalently four different models for the spatial distribution of the colloidal charge. First, we have considered a simple model where the charge is distributed uniformly (model 1),

$$\begin{aligned} \rho(r, z) &= \rho_0 \qquad \sqrt{r^2+z^2} < R \\ \rho(r, z) &= 0 \qquad \sqrt{r^2+z^2} > R, \end{aligned} \tag{S21}$$

where here and in what follows ρ_0 is a constant determining the charge density. Second, we have analysed a similar charge distribution as hypothesised in [6] for a colloid at an air-water interface, with the charge localised within a shell around the colloidal surface in the water phase (as $\epsilon_1 \gg \epsilon_2$) (model 2),

$$\begin{aligned} \rho(r, z) &= \rho_0 \qquad R - \delta < \sqrt{r^2+z^2} < R + \delta \text{ and } z < 0 \\ \rho(r, z) &= 0 \qquad \text{otherwise}, \end{aligned} \tag{S22}$$

with δ representing the half-thickness of the colloidal shell. A third model (model 3) is one where the charge is uniformly distributed inside the sphere, but there is charge dissociation outside, close to its surface. This is modelled by the following charge distribution,

$$\begin{aligned} \rho(r, z) &= \rho_0 & \sqrt{r^2+z^2} < R \\ \rho(r, z) &= \rho_0 e^{-\alpha(\sqrt{r^2+z^2}-R)} & \sqrt{r^2+z^2} > R, \end{aligned} \tag{S23}$$

and the motivation of this choice is to model charge dissociation effects close to the colloids, which are, for instance, suggested in [7] for a related but distinct system. Charge dissociation is also considered to be one of the main mechanisms through which charged colloids acquire their charge. Charge dissociation is here modelled as an exponential decay in the charge distribution, as arising due to the competition of a surface reaction and diffusion; α is the inverse length scale determining the decay of the charge distribution away from the colloidal surface, which is in general an independent lengthscale in our formulation (distinct from the Debye length). Finally, we have also considered charge

dissociation when the charge is localised in the colloidal shell in the water phase, as in the second model. The charge distribution in this final model (model 4) is given by

$$\begin{aligned} \rho(r,z) &= \rho_0 && R-\delta < \sqrt{r^2+z^2} < R \,\text{and}\, z<0 \\ \rho(r,z) &= \rho_0 e^{-\alpha(\sqrt{r^2+z^2}-R)} && \sqrt{r^2+z^2} > R \,\text{and}\, z<0 \\ \rho(r,z) &= 0 && \text{otherwise.} \end{aligned} \tag{S24}$$

The dielectric constant $\epsilon(r,z)$ equals ϵ_1 in the water phase ($\sqrt{r^2+z^2} > R$, $z<0$), $\epsilon_2 = \epsilon_1/40$ in the oil phase ($\sqrt{r^2+z^2} > R$, $z>0$) and inside the colloid ($\sqrt{r^2+z^2} < R$). The inverse Debye length is taken to be κ_1 in the water phase, κ_2 in the oil phase, and 0 inside the colloidal particle.

The two key dimensionless numbers determining the physics of the problem are [6] $\theta = \kappa_1 R$, the ratio between particle size and the Debye length in the water-like phase, and $\tilde{\sigma} = \frac{Qe_0}{\epsilon_1 R k_B T}$ the ratio between typical electrostatic energy and thermal energy, $k_B T$. In our system, to find the nominal colloidal charge Q we fitted the far field of the solution of the linearised version of Eq. (S20) via Eq. (11) in the main text (divided by Q to yield ϕ instead of U). We used this procedure because, as a consequence of the non-trivial form of the charge distributions, Q cannot be directly found by integrating $\rho(r,z)$ over space in general. For the models with charge dissociation (models 3 and 4), there is also a third dimensionless number, $\tilde{\alpha} = \alpha/\kappa_1$, quantifying the spatial decay of the dissociated charge profile. In our simulations, we fixed $\kappa_1 R = 1.2$, whereas other dimensionless numbers in Fig. 4 in the main text are: $\tilde{\sigma} = 394.89$ (Fig. 4A, model 1); $\tilde{\sigma} = 30.20$ (Fig. 4B, model 2); $\tilde{\sigma} = 143.30$ and $\tilde{\alpha} = 1$ (Fig. 4C, model 4). Figure S3 shows the result for model 3, with $\tilde{\sigma} = 119009$ and $\tilde{\alpha} = 2$ – the larger values of both parameter accentuates deviation from the Debye-Hückel theory. To gauge realistic parameter ranges, we note that for a colloidal sphere of $R \sim 1$ μm with a surface charge of $0.01 - 10$ μC/cm^2, $\theta \sim 1$ and $\tilde{\sigma} \sim 70 - 70000$; while $\tilde{\alpha}$ is not measured, the observations in Ref. [7] suggest that charge dissociation may occur over a micron-size lengthscale.

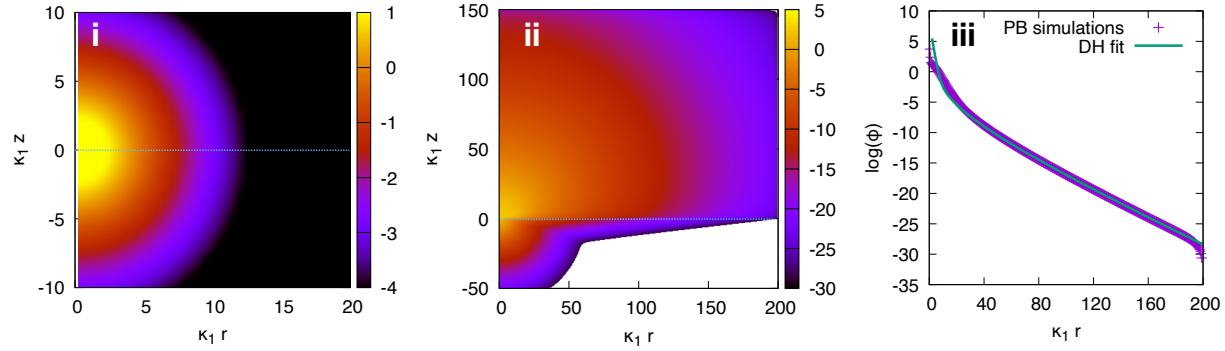

FIG. S3: Results of nonlinear PB simulations for a charged colloid with $\kappa_1 R = 1.2$ at an oil-water interface ($\epsilon_1 = 40\epsilon_2$, and $\kappa_1 = 10\kappa_2$). The charge distribution is uniform within the sphere, and there is also a charge distribution in both the oil and water phases which decays exponentially from the colloid surface (modelling charge dissociation, this is model 3 with $\alpha/\kappa_1 = 0.5$). (i) Heat map of the logarithm of the input charge distribution. (ii) Heat map of the logarithm of the electrostatic potential solving the nonlinear PB equation. (iii) Electrostatic potential on the interface ($z = 0$), as a function of r. The solid line is the fit to the Debye-Hueckel (DH) solution with an effective charge.

The PB solutions in Fig. S3 and in Fig. 4 of the main text show that the interfacial potential (at $z = 0$) is described well by the Debye-Hückel approximation in Eq. (S18) (divided by Q to yield the potential) for sufficiently large r, provided that we use an effective charge, Q_{eff}, which is different from the nominal charge Q (obtained, as mentioned previously, by fitting the Debye-Hückel solution to the linearised PB equation). [The small deviation close to $\kappa_1 r \sim 200$ is due to finite size effects due to the boundary conditions used.] In general, $Q_{\text{eff}} < Q$, as in [6] for an air-water interface. Specifically for the PB simulations presented in the main text and this Supplemental Material we obtain: $Q_{\text{eff}} = 0.39Q$ for model 1 (parameters as in Fig. 4A); $Q_{\text{eff}} = 0.98Q$ for model 2 (Fig. 4B); $Q_{\text{eff}} = 0.15Q$ for model 3 (Fig. S3); $Q_{\text{eff}} = 0.84Q$ for model 4 (Fig. 4C in the main text). The PB numerics also show that at low r the near-field behaviour of the system depends on the details of the charge distribution, and the crossover to the universal far-field behaviour occurs at different r for different models, and for different parameter values within the same model.

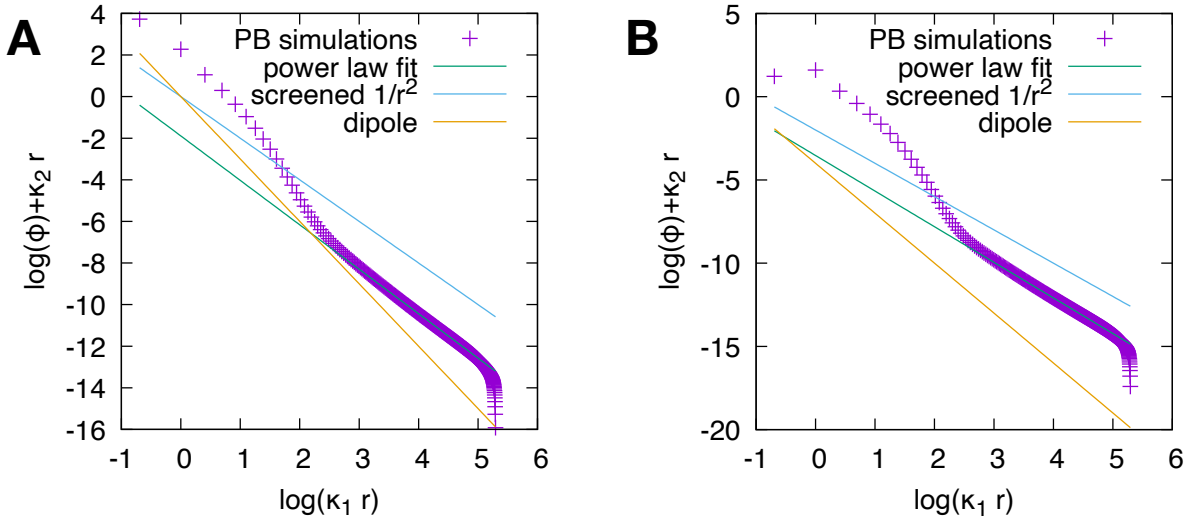

FIG. S4: Plot of the numerical solutions of $\log(\phi) + \kappa_2 r$ versus $\log(\kappa_1 r)$, showing that the asymptotic behaviour is given by a screened $1/r^2$ potential. For panel A, parameters are the same as in Fig. 4A in the main text; for panel B they are the same as in Fig. S3. The slopes, or effective exponents obtained by fitting the large r behaviour (before finite size effects kick in), are -2.14 and -2.15 for panels A and B respectively (which are compatible with the predicted asymptotic value of -2).

Comparison with experimental data

It is clearly of interest to compare the theoretical formula for interparticle interactions at an oil-water interface, Eq. (S18), to experimental results. To do so, we have analysed two sets of experimental data which we recently presented in [4]. These experiments recorded the force between two poly(methyl methacrylate)(PMMA) particles trapped at a dodecane-water interface, by using the blinking optical trap method (see [4] for more details). The first set of data was obtained by using poly(12-hydroxystearic acid) (PHSA) to sterically stabilise the particles, whereas the second set used poly(lauryl methacrylate) (PLMA) for stabilisation. In both cases, previous research showed that the colloids behave as charged particles at the interface [4]. To fit the force, we have compared a screened $1/r^2$ potential,

$$U_{\rm scr} = A\frac{e^{-\kappa_2 r}}{r^2}, \tag{S25}$$

where A and κ_2 were used as fitting parameters, with a dipole-dipole potential,

$$U_{\rm dip} = \frac{B}{r^3} \tag{S26}$$

with B the single fitting parameter.

Figure S5 shows the results from the screened $1/r^2$ and dipole fit (data correspond to $r \geq 7$ μm). Both potentials describe the data in an acceptable way in the range of distances which were probed by blinking optical traps. Quantitatively, however, the screened $1/r^2$ potential lead to a smaller value of reduced χ^2 [$\chi^2_{\rm red}$, note that this takes into account the different number of fitting parameters used in Eqs. (S25,S26)]. More specifically, the PMMA-PHSA fits yield ${\chi^2}_{\rm red} = 0.0097 \pm 0.0025$ for the screened $1/r^2$ potential, and to ${\chi^2}_{\rm red} = 0.0358 \pm 0.0079$ for the dipole, showing that the former gives a more accurate description of the data in the range probed experimentally. [Errors in ${\chi^2}_{\rm red}$ were computed by applying the bootstrap algorithm to the experimental data in all cases.] The difference in the two values of ${\chi^2}_{\rm red}$ is statistically significant (p value $p \simeq 0.002$). For PMMA-PLMA, again the screened $1/r^2$ fit ($\chi^2_{\rm red} = 0.0161 \pm 0.0035$) is better than the dipole fit (${\chi^2}_{\rm red} = 0.0404 \pm 0.0130$), although the statistical significance of the difference is smaller ($p \simeq 0.07$). The values of κ_2 obtained in the fits were $\kappa_2 \simeq 0.196$ μm^{-1} (PMMA-PHSA) and $\kappa_2 \simeq 0.046$ μm^{-1} (PMMA-PLMA), which should be compared with the value $\kappa_2 \simeq 0.1$ μm^{-1} expected for pure dodecane [4]. The results in Fig. S5 are interesting because the dipole fit is overall acceptable and this may explain why this theory has long been considered to be appropriate for interparticle interaction at an oil-water interface.

The experimental data are better fitted by the far-field asymptotic behaviour rather than by the full formula in Eq. (S18) (and by its analogue for the dipole case, $\kappa_2 = 0$, see Fig. S6A). This suggests that the near-field behaviour in experiments is different from that of ideal point-like particles. Interestingly, the experimental data are quantitatively

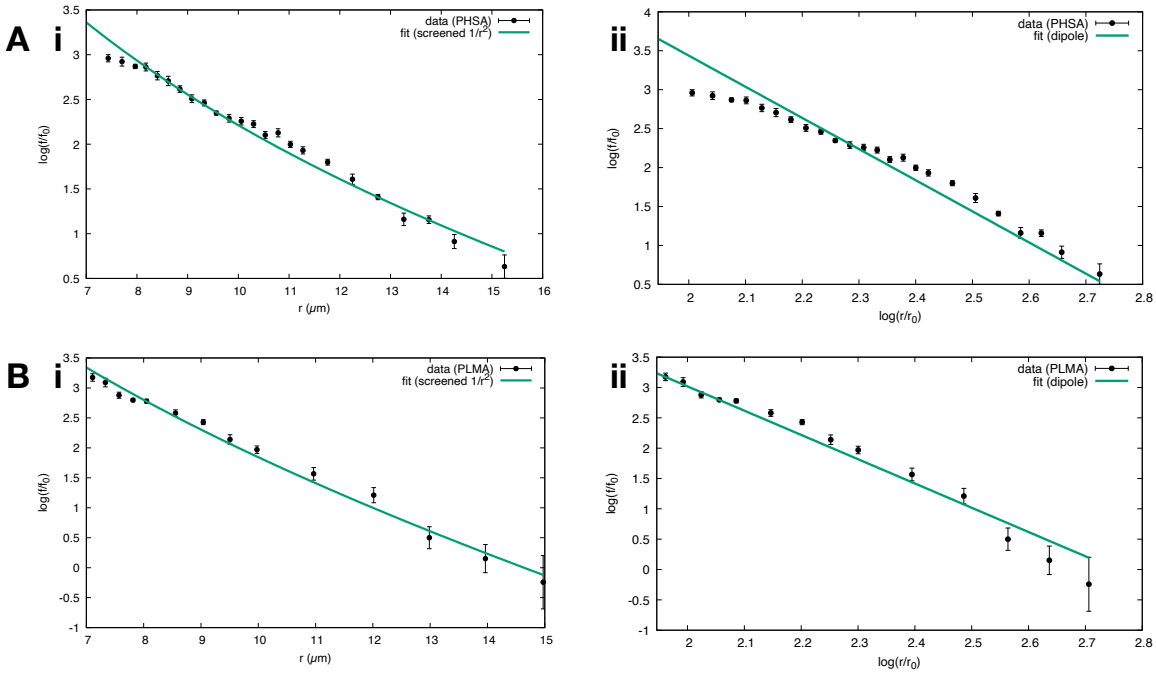

FIG. S5: Fits for blinking optical trap data for PMMA-PHSA (A) and PMMA-PLMA (B) with a screened $1/r^2$ [(i), Eq. (S25)] and a dipole [(ii), Eq. (S26)] potential. Note that curves correspond to force rather than potential; $f_0 = 1\ k_BT/\mu$m, $r_0 = 1\mu$m.

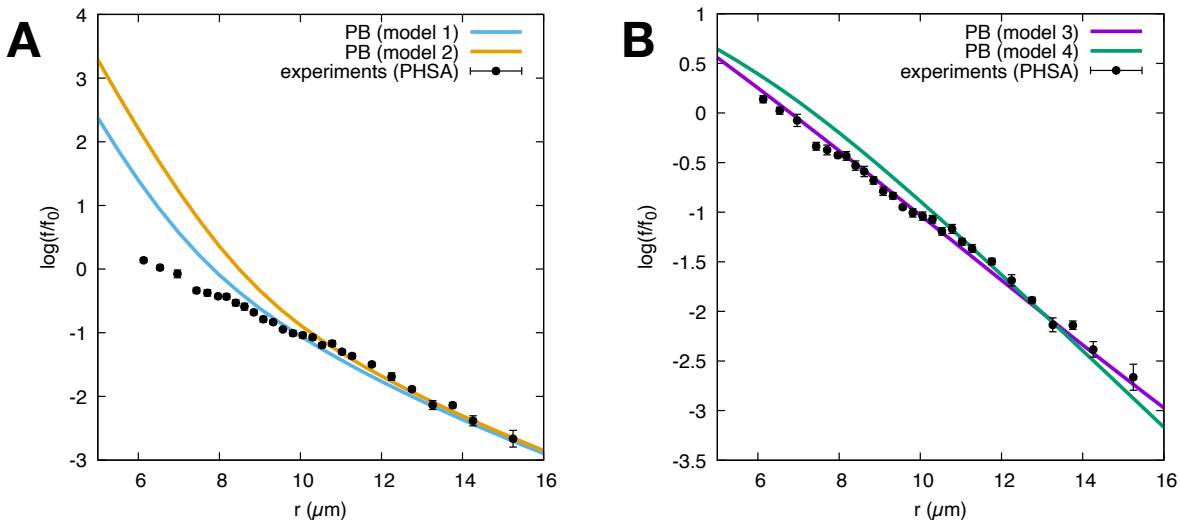

FIG. S6: Near-field and far-field behaviour in force versus distance curves for experiments (PMMA-PHSA) and simulations (models 1-4). (A) Models 1 and 2 poorly predict the near-field behaviour at low r. (B) Models 3 and 4 give force curves which are in better semiquantitative agreement with experiment. Curves have been shifted in the log axis by an arbitrary factor to ease comparison, so that f_0 depends on the curve. In (A) f_0 equals 1/300 $k_BT\kappa_1$ (model 1), 1/1600 $k_BT\kappa_1$ (model 2), $27k_BT/\mu$m (experiments). In (B) f_0 equals 1 $k_BT\kappa_1$ (model 3), 1/4 $k_BT\kappa_1$ (model 4), 27 k_BT/μm (experiments).

better described by our models with charge dissociation, models 3 and 4 (see Fig. S6B). While the semiquantitative comparison in Fig. S6 does not allow us to prove charge dissociation is the reason for the near-field behaviour probed experimentally, it serves to show that experiments can probe a range of interparticle distances where details such as particle size and charge distribution in principle matter.

Interfacial potential for a d-dimensional system: asymptotic behaviour

We now consider the case of a d-dimensional system (and a $(d-1)$-dimensional interface). The potential can be obtained by following the same procedure used in $d=3$ to be,

$$\begin{aligned}\phi(r) &= \frac{Q}{(2\pi)^{d-1}}\int d^{d-1}\mathbf{q}\frac{e^{i\mathbf{q}\cdot\mathbf{r}}}{\epsilon_1\sqrt{\kappa_1^2+q^2}+\epsilon_2\sqrt{\kappa_2^2+q^2}} \\ &= \frac{Q}{(2\pi)^{\frac{d-1}{2}}\,r^{d-2}}\int_0^\infty dx\frac{x^{\frac{d-1}{2}}J_{\frac{d-3}{2}}(x)}{\epsilon_1\sqrt{\kappa_1^2r^2+x^2}+\epsilon_2\sqrt{\kappa_2^2r^2+x^2}}.\end{aligned} \tag{S27}$$

To see that the two expressions in Eq. (S27) are equivalent, it is useful to note the following identity

$$\int_0^\pi \frac{d\theta}{2\pi}e^{iq\cos\theta}(\sin\theta)^n = 2^{\frac{n}{2}}\sqrt{\pi}J_{\frac{n}{2}}(q)\Gamma(\frac{n+1}{2}), \tag{S28}$$

where $n\geq 0$ is a non-negative integer.

We now study separately the case where $\kappa_1=\kappa_2$ (no interface, or bulk behaviour), and that of $\kappa_1\neq\kappa_2$, with both κ_1 and κ_2 non-zero.

A. $\kappa_1=\kappa_2$ case: the bulk Yukawa potential case

We start by analysing the behaviour of the following d-dimensional integral,

$$C_d = \frac{1}{(2\pi)^{d-1}}\int d^{d-2}\mathbf{q}_\perp\int_{-\infty}^{\infty}dq_\parallel\frac{e^{iq_\parallel r}}{\sqrt{\kappa^2+q_\perp^2+q_\parallel^2}}, \tag{S29}$$

which equals the interparticle potential in the bulk up to a multiplicative constant (equal to $\frac{Q^2}{2\epsilon}$). While this is well known, it is useful to solve this integral in a way which can be generalised to the interface case.

Introducing the $(d-3)$-dimensional unit sphere (i.e., the surface of a unit sphere embedded in a $(d-2)$-dimensional space), $S_{d-3}=\frac{2\pi^{\frac{d-2}{2}}}{\Gamma(\frac{d-2}{2})}$, and performing a "Wick rotation" in the $q_\parallel$ integral, equivalent to sending $q_\parallel\to iq_\parallel$, we obtain

$$\begin{aligned}C_d &= \frac{S_{d-3}}{(2\pi)^{d-2}}\int_0^{+\infty}dq_\perp q_\perp^{d-3}\int_{-\infty}^{\infty}\frac{dq_\parallel}{2\pi}\frac{e^{iq_\parallel r}}{\sqrt{\kappa^2+q_\perp^2+q_\parallel^2}} \\ &= \frac{S_{d-3}}{(2\pi)^{d-2}}\int_0^{+\infty}dq_\perp q_\perp^{d-3}\int_{+i\infty}^{-i\infty}\frac{idq_\parallel}{2\pi}\frac{e^{-q_\parallel r}}{\sqrt{\kappa^2+q_\perp^2-q_\parallel^2}} \\ &= \frac{S_{d-3}}{(2\pi)^{d-2}}\int_0^{+\infty}dq_\perp q_\perp^{d-3}\int_{-i\infty}^{+i\infty}\frac{dq_\parallel}{2\pi i}\frac{e^{q_\parallel r}}{\sqrt{\kappa^2+q_\perp^2-q_\parallel^2}}.\end{aligned} \tag{S30}$$

The integral over $q_\parallel$ is now equivalent to an inverse Laplace transform, whose asymptotic behaviour for $r\to\infty$ is dominated by its singularities, here a branchpoint at $q=-q_0\equiv-\sqrt{q_\perp^2+\kappa^2}$ (chosen so as to be able to close the Bromwich integration contour in the integral over $q_\parallel$ with paths in the complex plane over which the integral exists). Therefore, for $r\to\infty$, we obtain

$$C_d\simeq\frac{S_{d-3}}{(2\pi)^{d-2}}\int_0^{+\infty}dq_\perp q_\perp^{d-3}\int_{-q_0-i\infty}^{-q_0+i\infty}\frac{dq_\parallel}{2\pi i}e^{-q_0r}\frac{e^{q_\parallel r}}{\sqrt{2q_0}\sqrt{q_0+q_\parallel}} \tag{S31}$$

By using the inverse Laplace transform identity

$$\int_{-i\infty}^{+i\infty}\frac{dq_\parallel}{2\pi i}\frac{e^{q_\parallel r}}{\sqrt{q}} = \frac{1}{\Gamma(1/2)r^{1/2}} = \frac{1}{\sqrt{\pi}r^{1/2}} \tag{S32}$$

we get

$$\begin{aligned} C_d &\simeq \frac{S_{d-3}}{(2\pi)^{d-3/2} r^{1/2}} \int_0^{+\infty} dq_\perp q_\perp^{d-3} \frac{e^{-rq_0}}{\sqrt{q_0}} \\ &\simeq \frac{S_{d-3}}{(2\pi)^{d-3/2} r^{1/2}} \int_0^{+\infty} dq_\perp q_\perp^{d-3} \frac{e^{-r\kappa} e^{-\frac{rq_\perp^2}{2\kappa}}}{\sqrt{\kappa}}, \end{aligned} \tag{S33}$$

where in the last step we have approximated the integrand for $q_\perp \to 0$, as this will give the dominant contribution in the $r \to \infty$ limit. [Equivalently, we could have performed a saddle point approximation here.]

By rescaling $q_\perp$ and performing the final integral, we get

$$\begin{aligned} C_d &\simeq \frac{S_{d-3} 2^{\frac{d-2}{2}}}{(2\pi)^{d-3/2}} \frac{\kappa^{\frac{d-3}{2}} e^{-\kappa r}}{r^{\frac{d-1}{2}}} \int_0^{+\infty} dq_\perp q_\perp^{d-3} e^{-q_\perp^2} \\ &= \frac{2^{\frac{d}{2}-1} S_{d-3} \Gamma(\frac{d}{2}-1)}{2(2\pi)^{d-3/2}} \frac{\kappa^{\frac{d-3}{2}} e^{-\kappa r}}{r^{\frac{d-1}{2}}} \\ &= \frac{1}{(2\pi)^{\frac{d-1}{2}}} \frac{\kappa^{\frac{d-3}{2}} e^{-\kappa r}}{r^{\frac{d-1}{2}}}. \end{aligned} \tag{S34}$$

The resulting scaling is the well-known scaling of the d-dimensional Yukawa potential, or of the Gaussian correlator in the d-dimensional Landau-Ginzburg theory for the critical transition in a magnet [8].

B. $\kappa_1 \neq \kappa_2$ case

Asymptotics for the interfacial potential

We now consider the behaviour of the interfacial potential. For simplicity we set $\epsilon_1 = \epsilon_2 = 1$ (the asymptotic behaviour is the same as for $\epsilon_1 \neq \epsilon_2$). The potential is proportional to the following integral,

$$\begin{aligned} C_d &= \frac{S_{d-3}}{(2\pi)^{d-2}} \int_0^{+\infty} dq_\perp q_\perp^{d-3} \int_{-\infty}^{\infty} \frac{dq_\parallel}{2\pi} \frac{e^{iq_\parallel r}}{\sqrt{\kappa_1^2 + q_\perp^2 + q_\parallel^2} + \sqrt{\kappa_2^2 + q_\perp^2 + q_\parallel^2}} \\ &= \frac{S_{d-3}}{(2\pi)^{d-2}} \int_0^{+\infty} dq_\perp q_\perp^{d-3} \int_{-\infty}^{\infty} \frac{dq_\parallel}{2\pi} \frac{e^{iq_\parallel r}}{\kappa_1^2 - \kappa_2^2} \left[\sqrt{\kappa_1^2 + q_\perp^2 + q_\parallel^2} - \sqrt{\kappa_2^2 + q_\perp^2 + q_\parallel^2} \right] \\ &\equiv C_{d,1} + C_{d,2}. \end{aligned} \tag{S35}$$

As the second integral, $C_{d,2}$, describes propagation of the interaction in the second medium, and as $\kappa_2 < \kappa_1$, this will be the dominant contribution at large r. Performing a Wick rotation in the integral over $q_\parallel$, and using the following inverse Laplace transform identity (which involves regularisation of the integral),

$$\int_{-i\infty}^{+i\infty} \frac{dq_\parallel}{2\pi i} e^{q_\parallel r} \sqrt{q} = \frac{1}{\Gamma(-1/2) r^{3/2}} = -\frac{1}{2\sqrt{\pi} r^{3/2}}, \tag{S36}$$

we obtain

$$\begin{aligned} C_{d,2} &= -\frac{S_{d-3}}{(2\pi)^{d-2}(\kappa_1^2 - \kappa_2^2)} \int_0^{+\infty} dq_\perp q_\perp^{d-3} \int_{-\infty}^{\infty} \frac{dq_\parallel}{2\pi} e^{iq_\parallel r} \sqrt{\kappa_2^2 + q_\perp^2 + q_\parallel^2} \\ &= -\frac{S_{d-3}}{(2\pi)^{d-2}(\kappa_1^2 - \kappa_2^2)} \int_0^{+\infty} dq_\perp q_\perp^{d-3} \int_{-i\infty}^{+i\infty} \frac{dq_\parallel}{2\pi i} e^{q_\parallel r} \sqrt{\kappa_2^2 + q_\perp^2 - q_\parallel^2} \\ &\simeq -\frac{S_{d-3}}{(2\pi)^{d-2}(\kappa_1^2 - \kappa_2^2)} \int_0^{+\infty} dq_\perp q_\perp^{d-3} \int_{-i\infty}^{+i\infty} \frac{dq_\parallel}{2\pi i} e^{q_\parallel r} \sqrt{2q_0} \sqrt{q_0 + q_\parallel} \\ &= \frac{S_{d-3}}{(2\pi)^{d-2}(\kappa_1^2 - \kappa_2^2)} \frac{1}{2\sqrt{\pi} r^{3/2}} \int_0^{+\infty} dq_\perp q_\perp^{d-3} e^{-rq_0} \sqrt{2q_0} \\ q_0 &= \sqrt{q_\perp^2 + \kappa_2^2}. \end{aligned} \tag{S37}$$

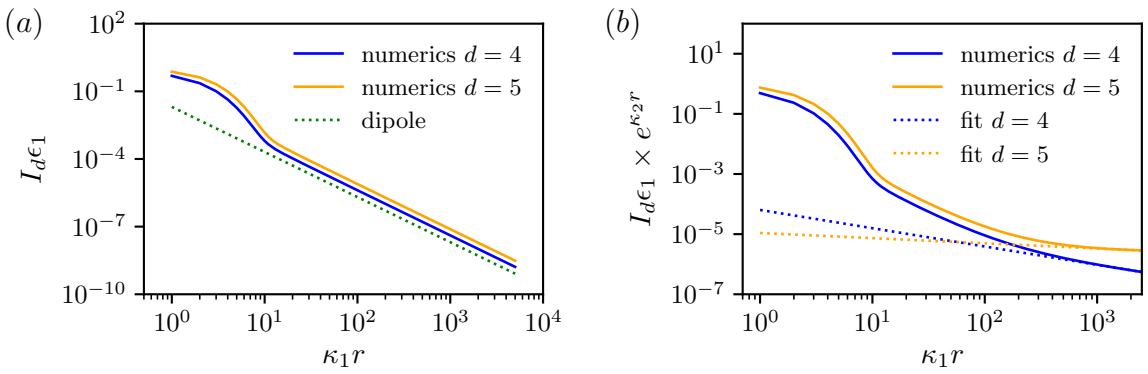

FIG. S7: (a) Log-log plot of the numerical solution of $I_d\epsilon_1$ versus $\kappa_1 r$ for $d = 4, 5$, $\epsilon_1 = 40\epsilon_2$ and $\kappa_2 = 0$. The decay corresponding to a dipole-dipole interaction is $1/r^2$ for any d, which is plotted as a dotted line. (b) Log-log plot of the value of $I_d\epsilon_1 e^{\kappa_2 r}$ versus $\kappa_1 r$ for $d = 4, 5$, $\epsilon_1 = 40\epsilon_2$ and $\kappa_1 = 100\kappa_2$. The dotted line denotes fit to power laws at large distances (see text).

As in Eq. (S33), we now approximate the integral over $q_\perp$ by noting that, for large r, it is dominated by the behaviour for $q_\perp \to 0$, to obtain

$$\begin{aligned} C_{d,2} &\simeq \frac{S_{d-3}}{(2\pi)^{d-3/2}} \frac{\sqrt{\kappa_2}}{(\kappa_1^2-\kappa_2^2)} \frac{e^{-\kappa_2 r}}{r^{3/2}} \int_0^{+\infty} dq_\perp q_\perp^{d-3} e^{-r\frac{q_\perp^2}{2\kappa_2}} \\ &= \frac{1}{(2\pi)^{\frac{d-1}{2}}} \frac{\kappa_2^{\frac{d-1}{2}} e^{-\kappa_2 r}}{(\kappa_1^2-\kappa_2^2) r^{\frac{d+1}{2}}}. \end{aligned} \tag{S38}$$

The resulting scaling coincides with that worked out previously for the special case of $d = 3$. It can be seen that for any $d \geq 3$ the limits $\kappa_2 \to 0$ and $\kappa_2 \to \kappa_1$ are both singular. The former limit gives zero, which means that a higher-order decay in r becomes relevant, and indeed $C_{d,2} \sim 1/r^{d-2}$ for $\kappa_2 \to 0$. The latter gives infinity, which means that the potential decays more slowly than in Eq. (S38), and indeed in that limit we obtain the bulk Yukawa potential in Eq. (S34).

Numerical results and fits

Figure S7 shows the results from numerically evaluating the integral in Eq. (S27), I_d, for $d = 4, 5$. In the limit in which $\kappa_2 = 0$, which is the d-dimensional analogue of an air-water interface, we obtain that $I_d \sim r^{-2}$, independent of d. Consequently, $\phi(r) \sim 1/r^d$ (Fig. S7a), which is the decay of an electrostatic dipole-dipole interaction in d dimensions. This is consistent with the physical picture that if one of the media is free from ions, the interparticle interaction is a repulsion between the dipoles which emerge as counterions in the aqueous phase assemble close to the point charges [2].

To approximate the interparticle interaction potential at the interface, $U(r)$, for cases in which $\epsilon_2 \ll \epsilon_1$ (as in oil-water interfaces), we can use a similar argument as done in the $d = 3$ case (see main text), but including only the small r and large r behaviours. We therefore fit the data with a sum of a Yukawa-like potential with decay constant κ_1, which should describe the behaviour at small distances, and the asymptotic behaviour in Eq. (S38) at large distances,

$$\frac{U(r)\epsilon_1}{Q^2} = A_d \frac{e^{-\kappa_1 r}}{r^{\frac{d-1}{2}}} + B_d \frac{e^{-\kappa_2 r}}{r^{\frac{d+1}{2}}}. \tag{S39}$$

The constants A_d and B_d can be set according to Eq. (S34) and Eq. (S38) respectively, or fitted as free parameters. Figure S8 shows the comparison between the numerical solutions for the interparticle potential in $d = 4, 5$ and the approximations (or fits) in Eq. (S39). The asymptotic behaviour is captured well by Eq. (S38); the Yukawa-like decay provides a poorer approximation at low distances, which is reasonable as in general in $d \neq 3$ Eq. (S34) is not exact, but is itself only asymptotically correct. Allowing A_d and B_d to be free parameters leads to a reasonable approximation for the numerical solution over the whole range of distances which we calculated.

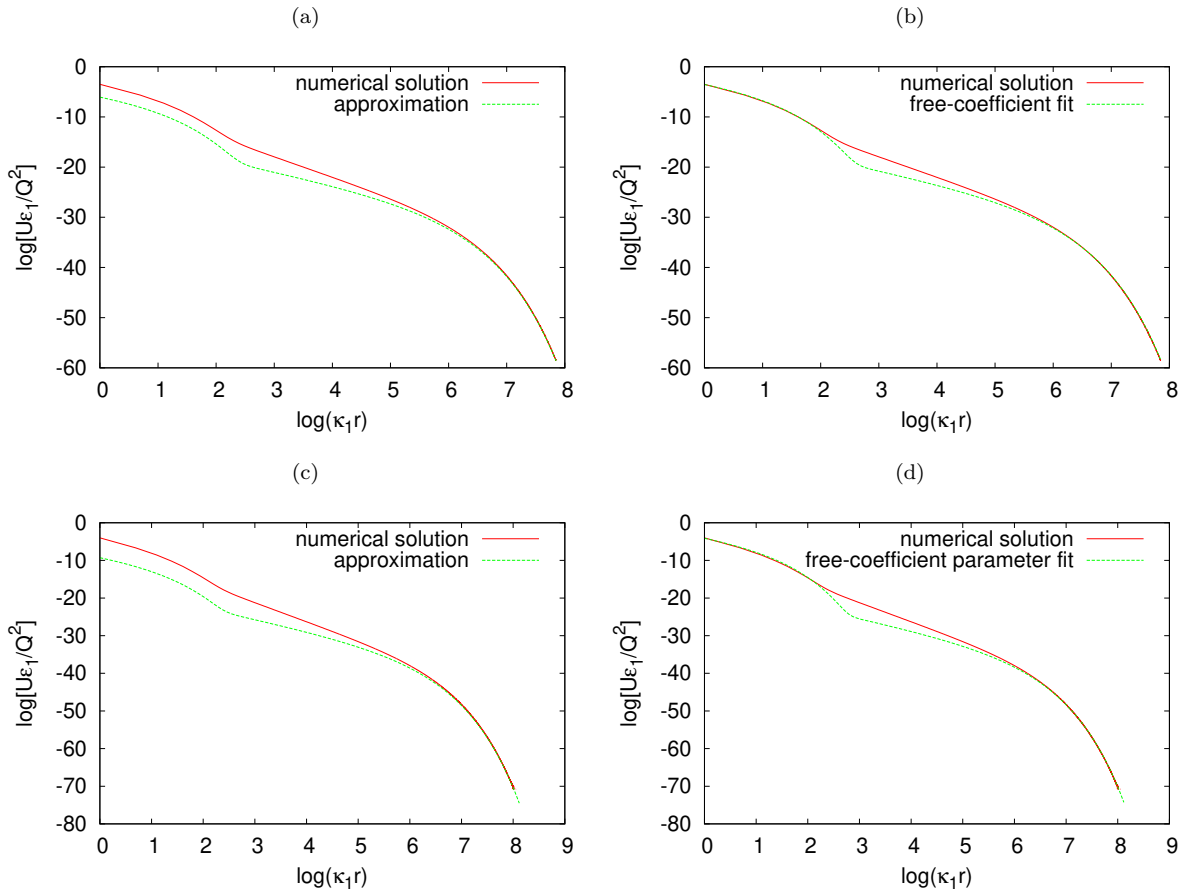

FIG. S8: (a) Comparison between the numerical solution for $U(r)\epsilon_1/Q^2$ versus r in $d = 4$ and Eq. (S39), with constants chosen according to the asymptotic analysis. (b) Comparison to a fit where A_4 B_4 were separately fitted to the low and high distances regimes respectively. The fit corresponds to Eq. (S39) with $A_4 \simeq 0.0779$ and $B_4 \simeq 2.02 \times 10^{-6}$. (c) Same as (a), but for $d = 5$. (d) Same as (b), but for $d = 5$. The fit corresponds to Eq. (S39) with $A_5 \simeq 0.0434$ and $B_5 \simeq 7.90 \times 10^{-8}$.

Additional numerical details

To evaluate the interparticle potential $U(r)$ (or the potential $\phi(r)$), we need to calculate the quantity I_d in Eq. (12) in the main text (equivalently the second row of Eq. (S27) in the SI).

As the integrands are highly oscillating functions, care needs to be taken in this numerical evaluation. For our purposes, we used the "quadosc" quadrature function in python. For $d = 3$, we split up the integration range between the zeroes of $J_0(x)$; for $d > 3$, we split up the range uniformly (with a period of 2π). [In $d = 3$, the methods are equivalent for the precision which we require.]

To solve the Poisson-Boltzmann equation, Eq. (S20), we have used a finite difference scheme in cylindrical coordinates. We used 400×400 grids in the simulations shown in Fig. 4 of the main text and Figs. S3,S4, and a spatial discretisation of $\Delta x = 0.5$ along both r and z. The time step in the relaxation algorithm was chosen to be $\Delta t = 0.15\Delta x^2$, which is small enough for the algorithm to converge, yet large enough to not compromise computational efficiency.

[1] F. H. Stillinger, Journal of Chemical Physics **35**, 1584 (1961).
[2] A. J. Hurd, Journal of Physics A **18**, L1055 (1985).
[3] M. Abramowitz, I. A. Stegun, *Handbook of Mathematical Functions* (New York) (1972).
[4] I. Muntz, F. Waggett, M. Hunter, A. B. Schofield, P. Bartlett, D. Marenduzzo, J. H. J. Thijssen, arXiv:1812.10299; *Phys. Rev. Res.* **2**, 023388 (2020).

[5] R. R. Netz, *Phys. Rev. E* **60**, 3174 (1999).
[6] D. Frydel, S. Dietrich, and M. Oettel, *Phys. Rev. Lett.* **99**, 118302 (2007).
[7] M. E. Leunissen, A. van Blaaderen, A. D. Hollingsworth, M. T. Sullivan, and P. M. Chaikin, *Proc. Natl. Acad. Sci. USA* **104**, 2585 (2007).
[8] P. M. Chaikin, T. C. Lubensky, *Principles of Condensed Matter Physics*, Cambridge University Press, Cambridge (1995).